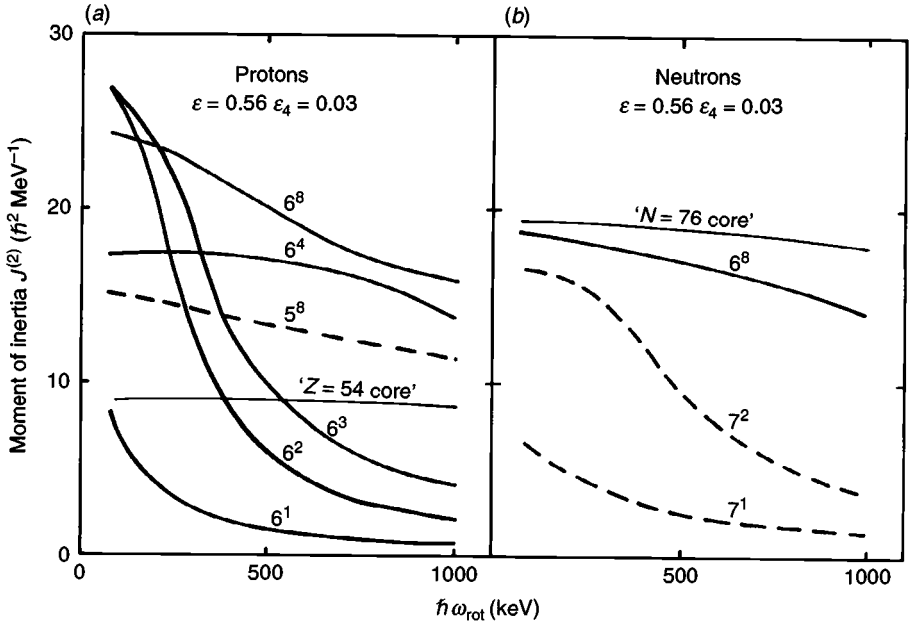

Fig. 12.21. At a deformation, typical for superdeformation in the $A = 150$ region, the contribution to the $\mathcal{J}^{(2)}$ moment of inertia from a) protons and b) neutrons in high-j shells is plotted versus the rotational frequency. The contribution from n particles in an N-shell is denoted as N^n. The lower orbitals in the $N = 6$ shell belong to $i_{13/2}$ and those in $N = 7$ to $j_{15/2}$ but as the j-shells are appreciably mixed at the large deformation, the labelling by N-shells is preferred. Furthermore, the contributions from a $(Z,N) = (54,76)$ core are shown. Note that this core contribution is essentially constant while large fluctuations are seen in the high-j part (from Bengtsson *et al.*, 1988).

the $\mathcal{J}^{(2)}$ moments of inertia are identical, i.e. when the spins are plotted versus transition energies (fig. 12.23), the slopes are identical. Near-identical superdeformed rotational bands have been found both in the Dy/Gd region and in the Hg/Pb region (see Janssens and Khoo, 1991, for a review). Furthermore, it has been noticed recently (Baktash *et al.*, 1992) that normal deformed rotational bands also have $\mathcal{J}^{(2)}$ values, which are surprisingly similar in many cases.

The surprisingly large number of identical bands might suggest that some 'new symmetry' is involved but no such symmetry is known at present. Indeed, we are far from a more general understanding of the identical bands. Even so, it seems appropriate to discuss some of the specific features and how they can be described in simple models. We will concentrate on the Dy/Gd region where the number of identical bands is rather small (at

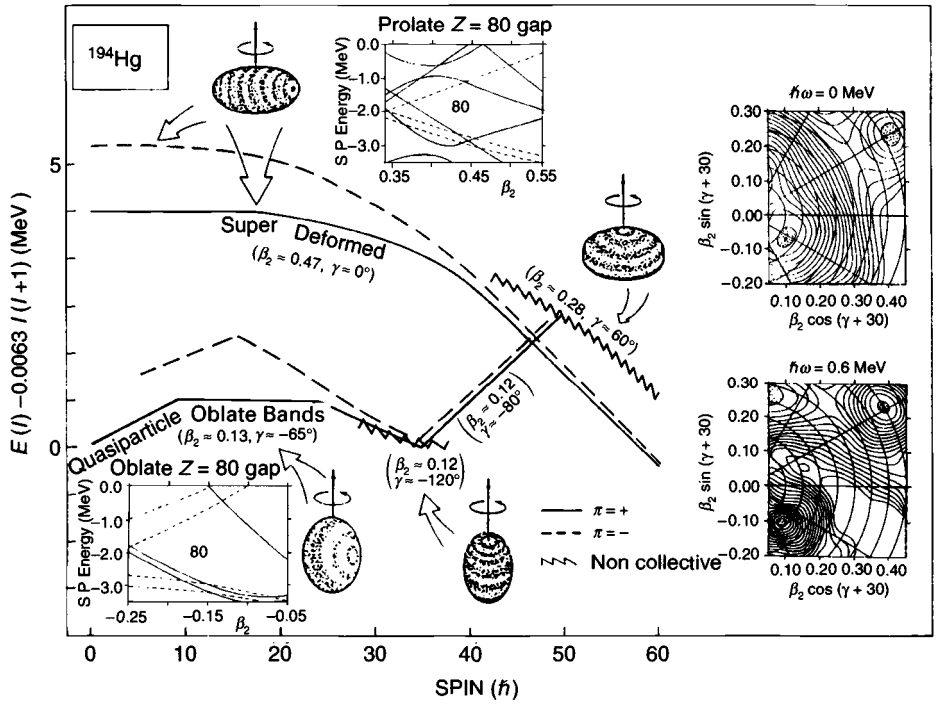

Fig. 12.22. Calculated excitation energy versus spin for ^{194}Hg illustrating a rich spectrum of collective and non-collective rotations, which evolve and co-exist near the yrast line. One insert shows the shell gap at oblate shape, which stabilises an oblate ground state configuration that terminates at prolate shape ($\gamma = -120°$) for spins just above $I = 30$. Another insert shows the $Z = 80$ gap at large prolate deformation, which is mainly responsible for the superdeformed configuration. Energy surfaces to the right indicate the corresponding minima at no rotation and at a high rotational frequency (M.A. Riley *et al., Nucl. Phys.*, 1990, **A512**, 178).

present) but those cases that have been observed are very distinct, extending over a large range of frequencies. This is illustrated in fig. 12.23 where the transition energies of ^{152}Dy are compared with those of superdeformed bands in neighbouring nuclei. The figure is drawn assuming specific values for the spins. If all the bands were shifted up or down by the same value in spin, this would change nothing in our conclusions. However, the relative spin assignments are crucial and although very reasonable, we must remember that they have not been measured.

The excitation energy versus spin, $E(I)$, for the superdeformed bands can (at least locally) be approximated by the parabola

$$E(I) \approx E_0 + AI(I+1)$$

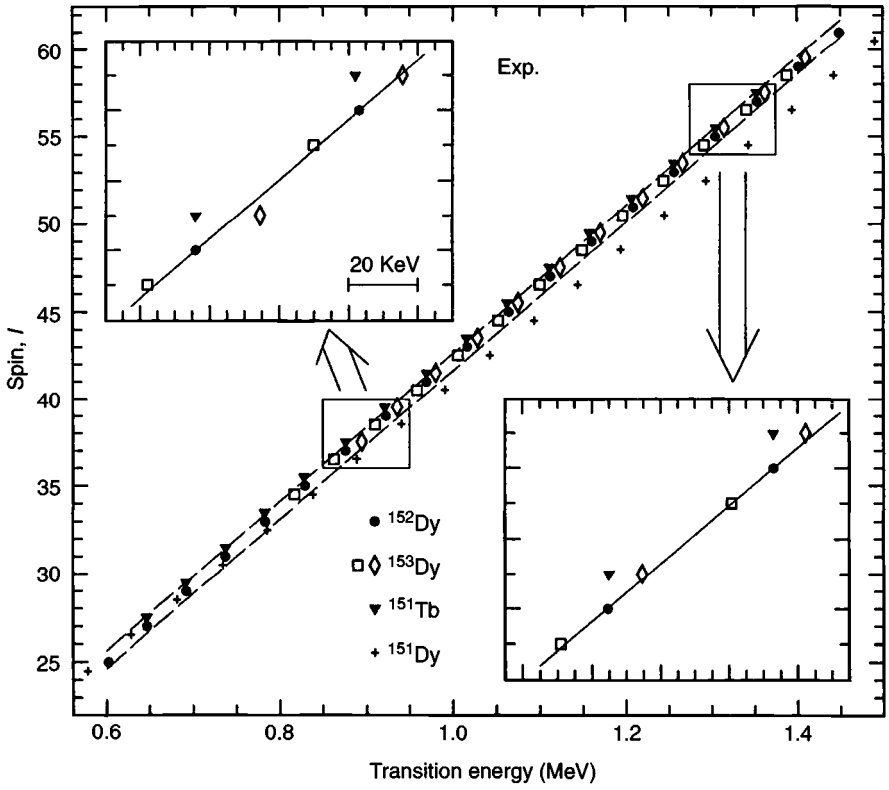

Fig. 12.23. Observed transition energies at superdeformation for ^{152}Dy, two bands in ^{153}Dy and the second band in ^{151}Tb. The bands are drawn as spin I versus transition energy E_γ. The functional dependence is very close to linear as indicated by straight dashed lines. In the insets, different parts are magnified with straight lines through the ^{152}Dy points. One finds that, within about 1–2 keV, the ^{152}Dy and ^{153}Dy data points (except one transition in ^{153}Dy) follow the same curve while the ^{151}Tb and ^{152}Dy data points have identical E_γ values. In the main figure, the ^{151}Dy data points are also included to show 'large' differences between superdeformed bands.

to a high accuracy. This means that the relation between the spin I and the quadrupole transition energies, E_γ, is approximately linear, namely

$$E_\gamma(I) = E(I+1) - E(I-1) \approx A(4I+2)$$

as comes out in fig. 12.23. Consequently, the energy difference between two consecutive transitions is roughly constant

$$\Delta E_\gamma(I) = E_\gamma(I+1) - E_\gamma(I-1) \approx 8A$$

Consider now the case that the excitation energy, $E(I) - E(I=0)$, is described by the same function for a rotational band in an even and an

odd nucleus. Then, when plotted as in fig. 12.23, all transitions will lie on the same line but because the spins are half-integer in the odd nucleus and integer in the even, the points of the two bands will be displaced relative to each other. Thus, with the even nucleus band as reference, the points in the odd nucleus will be displaced upwards or downwards by $\Delta E_\gamma/4$ depending on whether the spins in the odd nucleus are $0.5\hbar$ larger or smaller than the spins in the even nucleus.

It turns out that two bands in ^{153}Dy are identical to the yrast superdeformed band in ^{152}Dy in the way described here, i.e. that both the upward and the downward shift are realised. In fact, such bands come out from the most simple realisation of strong coupling discussed in chapter 11. In a simplified cranking model, assuming constant deformation and no pairing, such bands result if the orbital of the odd particle shows no alignment. This is easily seen if, starting from the cranking Hamiltonian, the expectation value with respect to the single-particle state $|\, i\rangle$ is taken:

$$e_i = e_i^\omega + \hbar\omega\langle j_x\rangle_i$$

With $\langle j_x\rangle_i = 0$, $e_i = e_i^\omega$ = constant, the total energy E_{sp} is changed by a constant while the total spin I remains unchanged (cf. fig. 12.24). When comparing two nuclei, an additional factor is that $\hbar\omega_{\mathrm{p}}$ and $\hbar\omega_{\mathrm{n}}$ depend on the number of protons and neutrons (chapter 8). This is, however, a small correction, see below.

For an orbital with $\langle j_x\rangle = 0$ independently of rotational frequency ω, the two branches with different signature will be degenerate but depending on in which of these orbitals the odd particle is put, the spin values realised are increased (signature $\alpha = 1/2$) or decreased (signature $\alpha = -1/2$) by $0.5\hbar$. Examples of orbitals that approximately fulfil the requirement of $\langle j_x\rangle = 0$ in fig. 12.16 are [303 7/2] in the $Z = 40$ region or [413 5/2], which is the 67th orbital at $\omega = 0$. For neutron particle states above '$N = 86$', the [402 5/2] orbital (cf. fig. 8.3) is of similar nature and could thus be responsible for the two bands in ^{153}Dy.

Even in more complete cranking calculations including shape polarisation, e.g. using the harmonic oscillator or the modified oscillator potential (see e.g. Ragnarsson, 1990; Szymański, 1990), it turns out to be rather easy to get out near-identical bands in calculations. Let us illustrate this by considering the rotating oscillator model in some detail. Thus, fig. 12.24 presents a comparison between calculated rotational bands in a 'core nucleus' (^{152}Dy) and 'core plus valence particle nucleus' (^{153}Dy), where the valence particle is placed in different orbitals. The differences between the calculated bands are illustrated as the difference between the I versus E_γ curves (of the type drawn

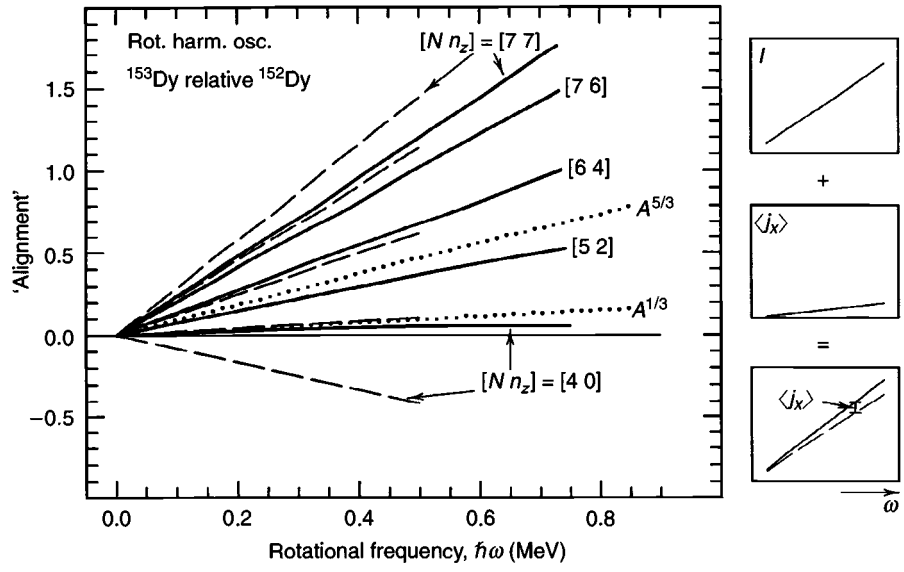

Fig. 12.24. Changes in transition energies ($E_\gamma = 2\hbar\omega$) caused by the addition of one particle to a core nucleus as calculated in the rotating harmonic oscillator. The core is defined from the asymptotic orbitals, which are filled in the superdeformed band of ^{152}Dy according to current theories. Its deformation is $\varepsilon = 0.57$. In the figures to the right is indicated schematically that, if a particle with alignment $\langle j_x \rangle$ is added to a core at constant deformation, this alignment (effective) is obtained from the differences in the I versus ω curves for the two bands. Thus, $\langle j_x \rangle$ as calculated from the simple expression given in section 12.2 is drawn by dashed lines for the orbitals considered (assumed to have $n_x = n_y$). Then we also give the calculated differences in transition energies (expressed as an effective alignment) between the core and the 'core plus particle' in a complete solution of the rotating oscillator. The important factors, in addition to the single-particle alignment, are the individual shape minimisation and the addition of an $A^{1/3}$ factor (see dotted line) because of the $A^{1/3}$-dependence of $\hbar\omega_0$. Note that the shape minimisation tends to 'decrease the scattering' between the different orbitals and that the average effect of all orbitals comes close to an $A^{5/3}$-dependence.

in fig. 12.23), i.e. as a relative alignment between the different bands. It is immediately obvious that, considered as functions of rotational frequency ω, all differences are essentially linear. Furthermore, with the valence particle in an equatorial orbital ($n_z = 0$), essentially identical bands are created while the bands in the two nuclei become increasingly different with increasing n_z of the valence orbitals.

In our simplified treatment of rotating oscillator (section 12.2), $\langle j_x \rangle \approx$ constant $\cdot\ \omega$. This relation and the relation $I = \mathcal{J} \cdot \omega$ for the core are illustrated to the right in fig. 12.24 and it is then also shown how they add. Thus, in this approximation assuming constant deformation, the difference between

the rotational bands is simply the alignment of the particle. Consequently, the alignments for the different orbitals are drawn in fig. 12.24. Then, in a complete treatment of the rotating oscillator there are additional effects. First, the oscillator constant $\hbar\omega_n$ varies with $A^{1/3}$ (and a $(N-Z)/A$ dependence, which is compensated by the sign change in the $(N-Z)/A$ dependence of $\hbar\omega_p$). This adds the same constant factor for all orbitals as illustrated in the figure. Second, the shape polarisation will change the moment of inertia of the core. Both of these corrections can be expressed as an effective alignment. The curves in fig. 12.24 are obtained from numerical calculation in the full rotating oscillator taking differences between calculated transition energies. It turns out, however, that the result would be almost the same if the different single-particle alignments curves were corrected by the change in rigid moment of inertia, $\mathcal{J}_{rig}$(core) $-\mathcal{J}_{rig}$(core+particle) due to the $\omega = 0$ shape change and by the $A^{1/3}$ factor. Thus, the main features of fig. 12.24 are easy to calculate analytically using the equilibrium deformations given in section 12.2.

One could also note from fig. 12.24 that, if a mean value of all orbitals is taken observing that there are more equatorial orbitals than polar orbitals, the result will be an approximate $A^{5/3}$-dependence as expected for a rigid moment of inertia. In more realistic nuclear potentials, the properties of the equatorial orbitals are about the same as in the pure oscillator. As these are the most common type of orbitals, one would expect a large number of identical bands at superdeformation from this point of view. On the other hand, one might question whether the approximation of pure single-particle motion in a mean field is realistic or not.

Coming back to fig. 12.23, if we accept the 'explanation' given above for the bands of ^{153}Dy that are identical to the band in ^{152}Dy, the other identity between the ^{152}Dy band and one band in ^{151}Tb is straightforward to explain although it appears even more strange at first sight. The fact is that, in this case, a rotational band in an even nucleus and a band in an odd nucleus have transition energies that are indeed *identical*, i.e. not displaced due to the different quantisation of the spin values. Within the scheme we have described, this is understood as caused by an orbital that shows an alignment already at no rotation, i.e. an $\Omega = 1/2$ orbital with a decoupling factor $a \neq 0$ (cf. section 11.2). For an equatorial orbital of this kind, the frequency-dependence of the alignment is essentially independent of the initial alignment. Thus, we can use the same arguments as above if we only add a constant factor corresponding to the $\omega = 0$ alignment. The identical transition energies in the bands in ^{152}Dy and ^{151}Tb then require an initial alignment of $\langle j_x \rangle = -0.5$ (corresponding to $|a| = 1$) for the active

orbital (the minus sign results because the particle is taken away, i.e. a hole excitation, when going from ^{152}Dy to ^{151}Tb). Indeed, in the single-particle diagram, the orbital [301 1/2] has essentially the desired properties even though the decoupling factor comes out somewhat smaller than $a = 1$ in most calculations using different potentials.

It was the observation (Byrski *et al.*, 1990) of the identical bands in ^{152}Dy and ^{151}Tb (and a similar identity between the yrast band in ^{151}Tb and one excited band in ^{150}Gd) that really focused attention on such bands (see e.g. Stephens *et al.*, 1990) and started a lot of theoretical investigations. This was so even though the identical bands in ^{152}Dy and ^{153}Dy were already known, as were also two identical superdeformed bands in the $A = 190$ region, the latter, however, over a range of fewer transitions. In the best cases, the identity of the transition energies is good within 1–2 keV extending over about 15 transitions with energies about 600–1600 keV. These numbers might, however, give the impression that the identity is even more strange than it really is. We must remember that all the superdeformed bands are very regular and follow essentially the same curve in an I versus E_γ diagram. This is illustrated in fig. 12.23 where we also give the transition energies for ^{151}Dy. The superdeformed band in ^{151}Dy is understood as being formed when one $N = 7$ neutron is removed from ^{152}Dy. Considering that these bands are found in neighbour nuclei, they are unusually different. This indicates that, if a more inert orbital is either empty or filled in two bands in neighbouring nuclei, the bands by necessity have to be rather similar. Even so, the extreme identity observed appears very strange. Furthermore, in view of the accuracy obtained in nuclear calculations in general, it is indeed surprising that the simple theories discussed here seem to describe the experimental situation so well. One would expect that different correlations not accounted for, especially pairing, would make the very detailed comparison between theory and experiment impossible. The models introduced here seem to be useful mainly in the Dy/Gd region. The superdeformed bands in the Hg/Pb region could not really be described within this scheme assuming pure single-particle degrees of freedom with no pairing. Different ideas on how the identical bands in Hg/Pb nuclei could be understood have been published e.g. by Stephens *et al.* (1990) and Azaiez *et al.* (1991). There is however no established understanding of these bands, see e.g. Baktash *et al.* (1993).

If the mechanisms for creating identical bands discussed here are qualitatively correct, it should also be possible to describe differences between bands that are not identical. One might say that to invent a theory which gives identical bands, or even bands that differ by some smooth quantity, is not

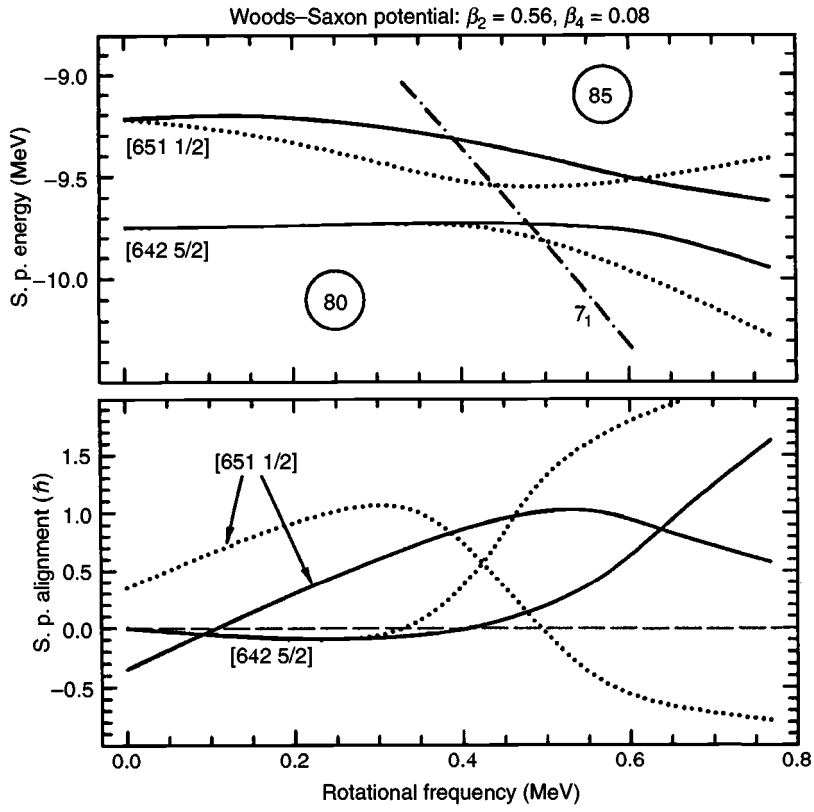

Fig. 12.25. The orbitals calculated in the Woods–Saxon potential at superdeformation in the $N = 80$–85 region are drawn versus rotational frequency ω in the upper figure while the alignments of the orbitals labelled by asymptotic quantum numbers [651 1/2] and [642 5/2] are shown in the lower figure.

so difficult. A better test of some theory is its ability to describe non-smooth differences between the observed quantities. Then, the superdeformed bands observed in $^{146-149}$Gd are especially favourable because some of these bands show a band-crossing while others do not.

When searching for orbitals at 2 : 1 deformations and neutron numbers $N = 82$–85, which could give rise to an observable crossing, the only reasonable candidates seem to be the $N = 6$ orbitals [642 5/2] and [651 1/2]. As should be evident from fig. 8.3, drawn for somewhat smaller deformations, these orbitals come close together for $\varepsilon = 0.5$–0.55. Other crossings occur between orbitals from different N-shells and appear to interact much less than observed in experimental bands. The details of this single-particle crossing are illustrated in fig. 12.25, as calculated in the Woods–Saxon

model. The single-particle orbitals are drawn in the upper figure where a very small energy interval is considered so that only the two signature branches of these two orbitals together with the lowest $N = 7$ orbital are seen (cf. fig. 12.16, which shows a much larger energy interval but where the crossings are drawn somewhat schematically. Consider e.g. the crossing between the [532 5/2] and [541 1/2] orbitals around $Z = 60$ in fig. 12.16 which in many ways is similar to the crossing in fig. 12.25). In the lower part of fig. 12.25, the alignments $\langle j_x \rangle$ of the orbitals are drawn. These alignments are proportional to the slopes in the upper figure.

In a way analogous to the identical bands, we now consider (Haas *et al.*, 1993) the differences between the transition energies of two bands in neighbouring nuclei with one orbital either filled or empty. For the orbitals of fig. 12.25, the calculated differences are drawn in the lower part of fig. 12.26. It is evident that this figure has the same structure as the alignments in fig. 12.25 and it is straightforward to see which orbital is either empty or filled when comparing two bands. The differences when comparing the two figures arise mainly from the fact that the Woods–Saxon potential has been used in one figure and the modified oscillator in the other. Furthermore, in fig. 12.26, we compare rotational bands which have been minimised in deformation independently while in fig. 12.25, the single-particle alignment $\langle j_x \rangle$ is shown. The comparison shows that, in the present formalism corresponding to single-particle motion in a mean field, it is the alignment of the specific orbitals which is the important factor and that e.g. deformation changes between different bands will only lead to minor corrections.

In the upper panel of fig. 12.26, the differences in transition energies between the observed bands are drawn. The large similarity between experiment and theory in fig. 12.26 seems to be very strong evidence that our interpretation of which orbitals are active is really correct. In drawing the experimental figure, one has to make specific assumptions about the relative spins but now it seems possible to turn the argument around, claiming that the good agreement between theory and experiment means that we have determined these relative spins. This would mean that, if it becomes possible to measure the spin values in one superdeformed band, we might extract the spins also for the bands in neighbouring nuclei. Indeed, in a recent paper (Atac *et al.*, 1993), it has been claimed that the spins in the superdeformed band of ^{143}Eu have been measured. At present, very few superdeformed bands are known in neighbouring nuclei of ^{143}Eu so it does not seem possible to carry out a similar analysis around ^{143}Eu as for $^{146-149}$Gd.

The cases we have chosen in fig. 12.26 are not really typical but more

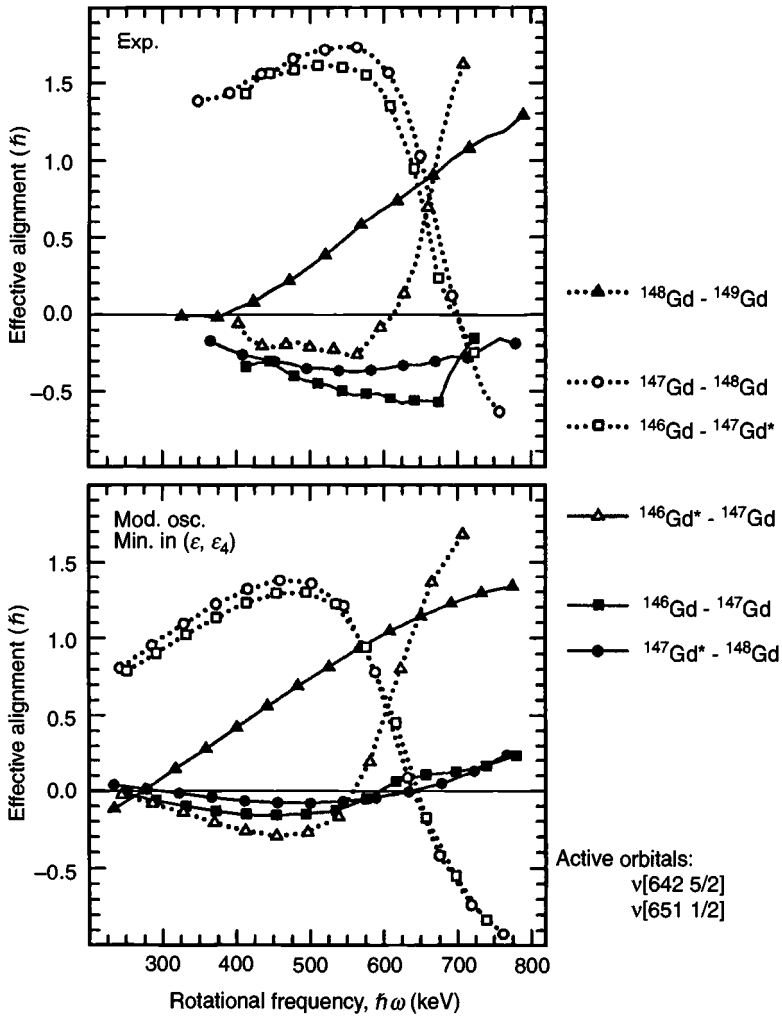

Fig. 12.26. The upper figure shows the relative transition energies for superdeformed bands in $^{146-149}$Gd where an asterisk indicates the 'second' band in that nucleus. The differences are plotted as (effective) alignments extracted as indicated in the lower right panel of fig. 12.24 ($\omega = E_\gamma/2$). Effective alignments extracted in the same way from rotational bands calculated in the modified oscillator are shown in the lower figure. A comparison with fig. 12.25 shows that it is the orbital that is labelled by [651 1/2] at $\omega = 0$ and has $\langle j_x \rangle > 0$ (the signature $\alpha = -1/2$ branch), which is being filled in the calculations when going from ^{147}Gd to ^{148}Gd or from ^{146}Gd to ^{147}Gd* etc. A comparison between the upper and lower figure strongly suggests a one to one correspondence between those orbitals used in the calculations and those active in the observed bands.

specific cases where theory and experiment seem consistent almost to the fine details. Even so, the comparison suggests that the superdeformed bands are really the best chance to see pure single-particle effects in nuclei. In the future, we could hope that a large number of rotational bands will be observed at different deformations (where favoured proton and neutron shell effects are 'in phase'). Thus, it might be possible to map the single-particle orbitals all the way from the ground state to two separated fragments. In this sense, nuclei are a very special laboratory in our study of quantum many-body physics.

Some more details of the cranking calculations have been reviewed in a recent paper (Bengtsson *et al.*, 1991) where also computer codes on a floppy disc are provided. The theoretical model behind the calculated energies shown in fig. 12.22 is somewhat different from the simple cranking model presented here. Specifically, the pairing interaction (chapter 14) is included. This should make the calculations more realistic in most cases but it has the disadvantage that they become less transparent and it becomes difficult to plot energy surfaces as functions of the physical quantity I or to follow the evolution of fixed configurations. Thus, the energy surfaces shown in fig. 12.22 are a mixture of different configurations (similar to fig. 12.8 for ^{160}Yb) and as they are drawn for a fixed rotational frequency, the spin I might be different at different deformations. Attempts to overcome these deficiencies have been made recently (Bengtsson, 1989). One could also note that, even within the simplified model described here, all the structures of fig. 12.22 come out (see calculations on ^{187}Au by Bengtsson and Ragnarsson, 1985) although in a somewhat qualitative way for low spins.

The recent discoveries of the superdeformed bands have thus made it possible to test theoretical predictions of the single-particle structure and the shell effects at large deformation. Fig. 12.15 suggests that favoured shell effects are present at large deformations for essentially all particle numbers. Thus, we would expect that, correlated with the particle number, rotational bands will be identified for essentially all deformations up to very elongated shapes, e.g. at 3 : 1 axis ratio. In this way it should be possible to scan large parts of fig. 12.15 and test how well the predictions are realised. One can then also start to ask more detailed questions about how large deformations and/or rotation disturb the nuclear quantal system.

Exercises

12.1 A particle of mass m is subject to the laws of classical mechanics. The motion of the particle can be described either in a laboratory